Beamtest of Non-irradiated and Irradiated ATLAS SCT Microstrip Modules at KEK

Y. Unno[1], T. Matuo[2], T. Hashizaki[2], T. Akimoto[8], J. Bernabeu[10], Z. Dolezal[4], L. Eklund[9], K. Hara[8], Y. Ikegami[1], Y. Iwata[5], Y. Kato[8], C. Ketterer[3], H. Kobayashi[8], T. Kohriki[1], T. Kondo[1], T. Koshino[2], J. Ludwig[3], T. Masuda[5], G. Moorhead[7], I. Nakano[2], K. Norimatsu[2], T. Ohsugi[5], K. Runge[3], S. Shinma[8], R. Takashima[6], R. Tanaka[2], N. Tanimoto[2], S. Terada[1], N. Ujiie[1], M. Vos[10], K. Yamanaka[5], and T. Yamashita[2]

[1]Institute of Particle and Nuclear Studies, High Energy Accelerator Research Organiation (KEK), Tsukuba 305-0801, Japan
[2]Physics department, Okayama University, Okayama 700-8530, Japan
[3]Department of Physics, Albert-Ludwig University of Freiburg, D-79104 Freiburg, Germany
[4]Institute of Particle and Nuclear Physics, Charles University, CZ-180 00 Prague 8, Czech Republic
[5]Physics department, Hiroshima University, Higashi-Hiroshima 739-8526, Japan
[6]Education department, Kyoto University of Education, Kyoto 612-0863, Japan
[7]School of Physics, University of Melbourne, Parkville, Victoria 3052, Australia
[8]Institute of Physics, University of Tsukuba, Tukuba 305-8571, Japan
[9]Department of Radiation Science, Uppsala University, S-75121 Uppsala, Sweden
[10]Institute Fisica Corpuscular, Universidad de Valencia, E-46017 Valencia, Spain

Abstract

Non-irradiated and irradiated ATLAS SCT barrel and forward modules were beamtested with 4 GeV/c pions. Pulse shapes confirmed the peaking time of the amplifier to be 22 ns and deteriorated slightly in the irradiated modules. Median charges saturated around 3.8 fC both in the non-irradiated and irradiated modules. Signal/Noise ratios, using the noises from the in-situ calibration, were >16 in the non-irradiated (>150 V), and >10 in the irradiated (>300 V) barrel modules. No excess common-mode noise was observed.

I. Introduction

In order to investigate the origin of the mass of elementary particles and new physics of the universe, the accelerator, LHC (Large Hadron Collider), is being built at CERN which accelerates and collides protons at the centre of mass energy of 14 TeV, with a collision luminosity of 10^{34} $cm^{-2}sec^{-1}$ and a beam crossing interval of 25 ns. Two major experiments, ATLAS and CMS, are under construction, both being aiming to detect all possible charged and neutral particles emerging from the fundamental interactions.

In the ATLAS experiment, the detection and the measurement of momentum of charged particles are made in the inner detector, consisted of pixel (PIXEL), silicon microstrip (SCT) [1], and transition-radiation (TRT) detectors, inside a 2 Tesla solenoid magnet of a diameter of 2 m in the centre of the ATLAS detector complex. The SCT provides high-precision tracking information with a position resolution of 23 μm per sensing planes. The central barrel section is made of 4 cylindrical and the forward-backward section of 2x9 disk layers, where one layer is formed with two sensing planes. The area of silicon sensing plane is 34 and 27 m^2 in the barrel and the forward-backward sections, respectively. The silicon microstrip sensors are to receive a cumulative fluence of $2x10^{14}$ 1 MeV-neutron-equivalent particles/cm^2 over 10 years of operation at the inner-most radius of 30 cm from the collision axis.

The barrel and the forward-backward sections are covered with detector units called “module”s made of silicon microstrip sensors and the fast-shaping on-off readout electronics, combined with electrical, mechanical, and thermal structures. After intensive development from the technical design report [2], the full-size SCT modules, fully equipped with SCT-specified components, have become available, including those irradiated to the full fluence of particles.

Two beamtests [3] were carried out at KEK using pion beams of 4 GeV/c at its 12 GeV proton synchrotron, for measuring the performance of the fully equipped SCT modules in an environment of experiment. These were the first beamtests of the SCT modules, succeeding the beamtests of components [4]. Since the results of the second beamtest covered the results of the first test, only those of the second test were presented in this paper.

II. SCT silicon microstrip modules

A. ATLAS SCT silicon microstrip sensor

After intensive studies of the radiation damage and developments of radiation-tolerant designs, ATLAS SCT has chosen a type of silicon microstrip sensors of p-implant strips in the n-bulk silicon wafers, so-called p-in-n sensors. One type of sensor, square, is used for the barrel modules and 5 types of wedge sensors for the forward-backward (abbreviated as “forward”) modules. The sensors are designed to have a mean strip pitch of 80 μm at the centre of a module. The parameters of the barrel and the forward sensors used in the beamtest are summarized in Table 1 [5].

B. Frontend readout ASIC

The signals from the strips are read out with a frontend electronics with high gain (50mV/fC), unipolar fast shaping (20 ns

·Manuscript draft Nov. 4, 2001. This work was supported in part by the Grant-in-aid for Scientific Research of Japan Ministry of Education, Science, and Technology, Australian Research Council, and BMBF (German Ministry for Education and Research).

Table 1
Parameters of the ATLAS SCT p-in-n silicon microstrip sensors

Module	Barrel	Forward
Sensor type:	p-in-n, AC-coupled, Single-sided	
Thickness:	285 ± 15µm	
Shape:	square	wedge
Size (outer) (width×length):	63.6mm×64.0mm	71.8/64.7mm×57.5mm 64.6/56.5mm×65.5mm
Bulk:	n-type, high resistivity (about 4 kΩcm)	
Strip type:	p^+	
Strip pitch:	80 µm	85.95, 77.45 µm
Strip length:	62 mm	55.5, 63.5 mm
Strip width:	22 µm	
Number of strips:	768 readout + 2 shaping	
Strip AC coupling:	SiO2 + SiN, >20 pF/cm	
Backside:	Uniformly doped n^+ layer	

peaking time), on-off discriminating (binary), and buffering the digitized bits for 3.3 µs duration. The SCT specific design, named ABCD, is implemented in a BiCMOS single chip application-specific-integrated-circuit (ASIC) in a radiation-tolerant technology [6]. One ASIC is made of 128 channels.

After the first generation design, the second generation ABCD2T implemented a 4 bit DAC in individual channels to reduce excess threshold spread (trim DAC), and shielding the input pads for excess noise protection [7]. The third generation ABCD3T fixed a poor matching in the circuit which generated the correction voltage for the discriminator threshold, and added a 2-bit range for the step of the trimDAC to cope with the deteriorated trimming offset spread after irradiation [8].

C. Barrel and forward modules

The SCT modules are designed to have a strip length of 12 cm and two coordinate sensing in a module. A pair of sensors are glued on the top and the bottom of a baseboard at an angle of 40 mrad. A module is equipped with 12 ABCD chips on a hybrid, 6 on the top and 6 on the bottom side. The hybrid is placed near the centre of the module in the barrel modules, wrapping around, and at the end in the forward modules, double-sided. The designs are driven principally by the difference in cylindrical and disk geometries. Photographs of the barrel and forward modules are shown in Figure 1 and Figure 2.

A thermal management is critical in order to extract the heat of the ASICs (5 to 8 W), and of the sensors, specially of the radiation-damaged sensors (1 to 2 W). The baseboard with a high thermal conductivity is a key element in order to prevent the thermal runaway of the sensors. The barrel module is cooled in one area at the wide tab and the forward module in two areas: one at the junction of the sensor and the hybrid and the other at the far-end of the sensors.

Two modules, one barrel and one forward, were irradiated prior to the beamtest to the fluence of $3x10^{14}$ protons/cm^2 at the 24 GeV proton synchrotron at CERN, equivalent to the $2x10^{14}$ 1 MeV neutrons/cm^2. The modules were annealed for 7 days at

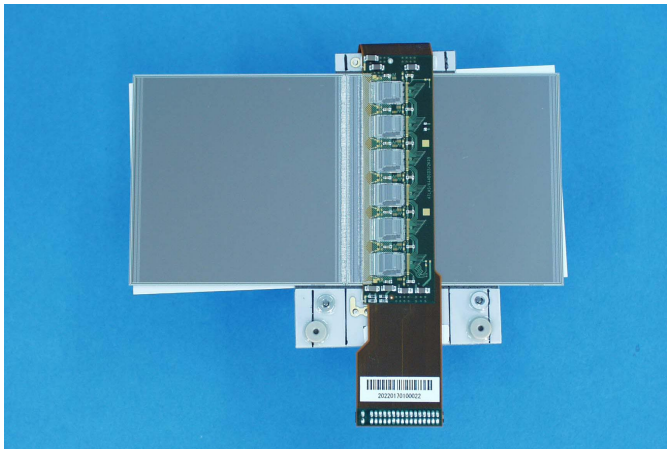

Figure 1: ATLAS SCT barrel module

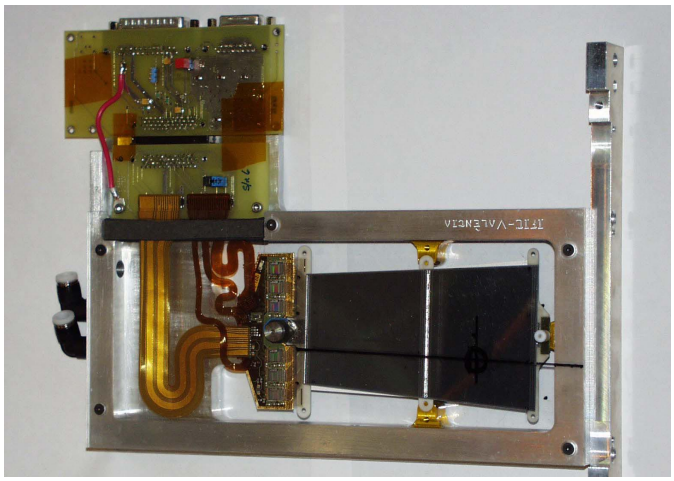

Figure 2: ATLAS SCT forward modules, together with a module frame and a readout card of the beamtest

28 °C, in order to simulate the effects of the warm-up for the maintenance in the real experiment, and placed for several days in the room temperature for preparation. Otherwise they were kept cold (<-10 °C).

III. BEAMTEST

A. Setup

Two beamtests were carried out. Two barrel and one forward modules with ABCD2T chips were tested in the first, and three barrel and three forward modules with ABCD3T chips, including two irradiated modules, were tested in the second beamtest. A classification of the modules is summarized in Table 2 [9].

The modules were attached to aluminium module frames and positioned in a thermo-box in the beamline. Three “Si-telescopes” were placed, in sandwiching two modules in between, in order to provide a position resolution of about 5 µm in hori-

Table 2
Name, type, ASIC, and irradiation characteristics of the modules in two beamtests

Beamtest		Name	Type	ASIC	Irradiation
1		k3103	barrel	ABCD2T	non-irrad
		FR-k81	forward	ABCD2T	non-irrad
		k3104	barrel	ABCD2T	non-irrad
2	mod1	011	barrel	ABCD3T	non-irrad
	mod2	022	barrel	ABCD3T	non-irrad
	mod3	003	barrel	ABCD3T	irrad
	mod4	VAL-k3-166	forward	ABCD3T	irrad
	mod5	VAL-k3-165	forward	ABCD3T	non-irrad
	mod6	CG-k3-170	forward	ABCD3T	non-irrad

zontal and in vertical directions. The modules were separated by 30 mm each other. The smearing by multiple scattering was estimated to be negligible by interpolating the positions of the incident particles with two adjacent telescopes. The incident particles were triggered with the scintillators of 2 cm x 2 cm placed in the upstream.

The modules were cooled in two ways: the overall environment inside the thermo-box was cooled with a circulation of cold air of about -20 °C, and, in addition, the irradiated modules were cooled with a liquid cooling of about -13 °C. The temperatures of the barrel hybrid were about 0 °C.

The temperatures of the sensors were estimated to be about -10 °C. The typical leakage currents of the non-irradiated and the irradiated modules were 0.2 μA and 2 mA, respectively. The forward modules had trouble in cooling the hybrids and the temperatures were about 37 °C and 54 °C in the non-irradiated and the irradiated modules.

B. Trim range setting in the irradiated modules

After the irradiation, ABCD3T chips showed a problem in setting the trim DAC range of the trim circuitry. (This problem was fixed in the latest ABCD3TA chips.) The ranges were stuck to 1 and 2 in mod3 and 2 and 3 in mod4, in the 4 chips where the beam particles passed (beam spot). The resulting masked channels which were out-of-trimming were, however, small: 1 and 4 channels in the mod3 and the mod4 modules, respectively.

C. Charge calibration

The relations of the threshold voltages and the charges were calibrated, in situ, by injecting charges with the internal circuitry in the ABCD chips. The resulting calibration curves, averaged over the chips in the beam spot, are shown in Figure 3.

The internal calibration circuitry required several correction factors: deviation of the capacitance values of the charge injection capacitors, deviation of charge scales due to the chip temperatures and radiation damages. These factors were measured and/or estimated as in Table 3. The charge scales were multiplied by the Total factors.

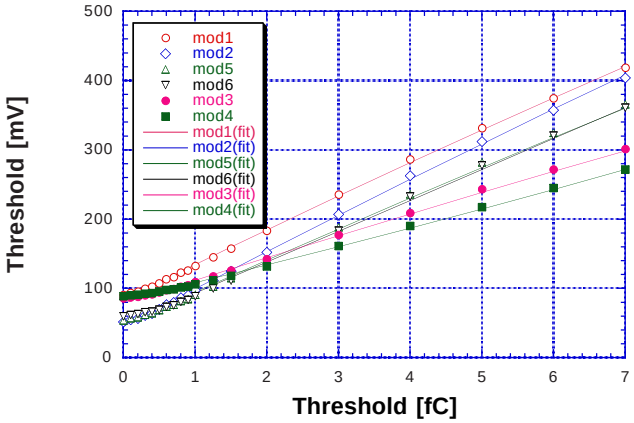

Figure 3: Calibrations of the threshold in mV and fC

Table 3
Charge correction factors due to calibration capacitance (Cap), temperature (Temp), irradiation(Irrad), and combined total(Total)

mod	Name	Cap	Temp	Irrad	Total
1	011	1.07	1	1	1.07
2	022	1.07	1	1	1.07
3	003	1.07	1	0.97	1.04
4	166	1.07	0.95	0.97	0.99
5	165	1.07	0.97	1	1.04
6	170	1.07	0.97	1	1.04

D. Data taking and analysis

Data were taken by varying two parameters: the sensor bias voltage between 25 and 275 V for the non-irradiated and 150 and 500 V for the irradiated modules, and the threshold between 0.7 and 6 fC. In the following analyses, the conditions taken for a typical setting were, otherwise mentioned, (1) bias voltages of 150 V and 350 V for the non-irradiated and the irradiated modules, and (2) threshold at 1 fC. In the plots, the voltages of the irradiated modules were corrected for the voltage drops in the series resistance in the bias supply lines.

IV. Data Analysis

A. Pulse shape reconstruction

The ABCD chip has a discriminator circuitry with two modes. One of them is a sampling at the phase of the clock. With an externally supplied self-running clock, the signal pulses, after the amplification and shaping, are sampled continuous-

ly since the arrival time of particles and the clock phase is random. Combining the threshold scanning and the measurement of the time between the triggers and the clock phase, the time distribution of the median pulse heights can be reconstructed.

The ABCD chips were clocked at 40 MHz and the time between the triggers and the clock phase were measured with a TDC in the beamtest. The resulting time distributions of the median pulse heights are shown in Figure 4 for the non-irradiated (average of mod1 and mod2) and for the irradiated (mod3) modules. The positions of the peaking were adjusted to be at 40 ns. The impulse response curves of a first-order differential and third-order integration circuitry, CR-RC^3, were fitted in the rising part of the pulses, between 20 and 45 ns. The peaking time of the non-irradiated module was 22 ns and that of the irradiated one was 27 ns. The peaking time of the non-irradiated chips was consistent with the ABCD specification. The peaking time of the irradiated module was slower due to a slower charge collection in the radiation-damaged sensors and a slower speed of the damaged amplifiers.

Other distinctive feature of the reconstructed pulses was the shoulders seen after the peaking. This shoulder could not be reproduced in the simulation of the charge collection in the damaged sensors. Since the shoulder was said not observed in the chips without the discriminators [10], this would be a physical feedback of the discriminator shocks. Compared to the barrel modules, larger excess shoulders were observed in the forward modules.

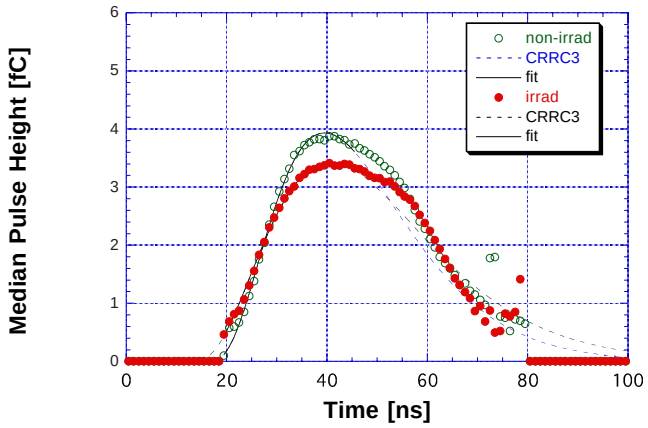

Figure 4: Median pulse height distributions as a function of time to the triggers: non-irradiated (open circle) and irradiated (filled circle) modules, and the impulse responses of CR-RC^3 circuitry (solid line being the fitted region) with the peaking times of 22 and 27 ns, respectively

The peaking times of the modules as a function of bias voltages were shown in Figure 5. In the non-irradiated modules, the pulses slowed down slightly, by 3 ns, below 150 V to 50 V. The forward modules were slower than the barrel modules, by 5 ns in the non-irradiated and 7 ns in the irradiated modules. These deterioration might be caused by the higher temperature of the chips in the forward hybrids.

In the following analyses, an event selection was applied to those events which time was in the peak region, between 35 and 45 ns. No correction was made to the range in other bias voltages since the move of the peak position was small.

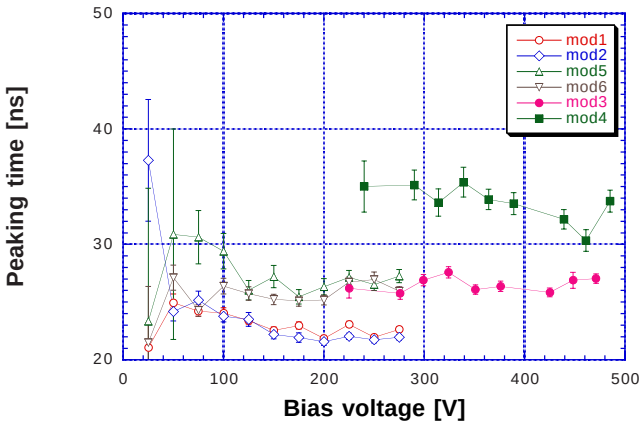

Figure 5: Bias voltage dependence of the peaking times

B. Position resolutions

In a sensing plane of a module, consecutive hit-strips were clusterized to define a hit-cluster, with the geometrical centre as the position of the “cluster centre” and the number of strips as the “cluster width”. The trajectories of the incident particles were made with two adjacent telescopes in order to minimize the effect of multiple scattering. The deviations of the cluster centres from the trajectories were the position resolution of the sensing plane.

The deviation distributions of the module, mod1, is shown in Figure 6, for all events (circle) and for the cluster width greater than 1, the “multi-hits”, (diamond). The distribution of all events is close to the uniform distribution of the pitch, 80 µm. That of the multi-hits is much narrower due to the fact that the multi-hits occurs where the particles hit in the midway between the strips, effectively reducing the width of the sensitive region.

In order to derive the root-mean-square (RMS) resolution of the uniform distribution, the Gaussian functions were fitted, without weighting, and the Gaussian sigma was reduced by a factor 1.24 associated to the difference in the RMS and the Gaussian standard deviations when fitted to the uniform distribution. The resulting RMS resolutions were 22.5 µm and 10 µm for the all and multi-hits events, respectively.

In analysing the forward modules, a correction to the fan geometry was taken into account to project the hit at t=(x, y) to the x axis defined at a pitch, p, approximated as

$$xp = x + ((d\theta)/(dx)) \cdot x \cdot y\,. \qquad (1)$$

The pitch evaluated was 86 µm where the beam spot was.

The RMS resolutions are shown in Figure 8 and Figure 9 as a function of bias voltage and threshold. Those of the modules

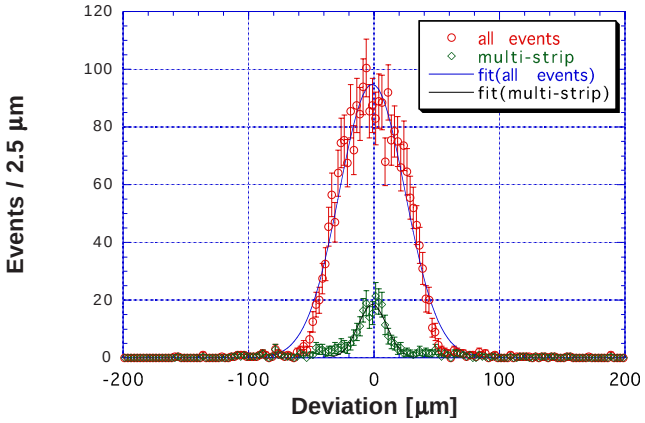

Figure 6: Deviations of the cluster centre from the expected positions of incident particles of the mod1 module: all events (circles) and the events with multi-hits (diamonds), with Gaussian fits, without weighting

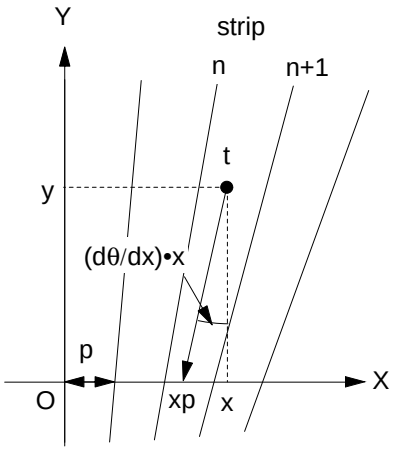

Figure 7: Correction of the fan geometry. A hit at t=(x,y) is projected at the hit x1 at the x-axis of the pitch p, approximated as xp=x+(dθ/dx)•x•y

outside the telescopes were corrected for the multiple scattering effect. The RMS resolutions of the barrel and the forward modules were about 23 µm and 26 µm, consistent with the pitch of 80 µm and 86 µm, respectively, although those of the forward modules were slightly worse than the expected.

In the bias voltage dependence, there was very little dependence in the non-irradiated modules, while those of irradiated modules showed an improvement by reducing the bias voltage. The dependence on the threshold was a bit complicated: both below and above 1.5 fC the resolutions were improved. These can be understood as the combined effect of fraction of multi-hits and the loss of efficiency where the former increases events in narrow distributions while the latter reduces the sensitive widths.

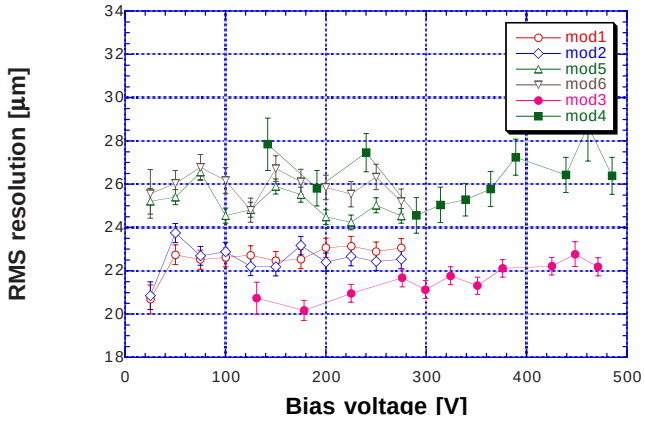

Figure 8: RMS resolutions as a function of bias voltage.

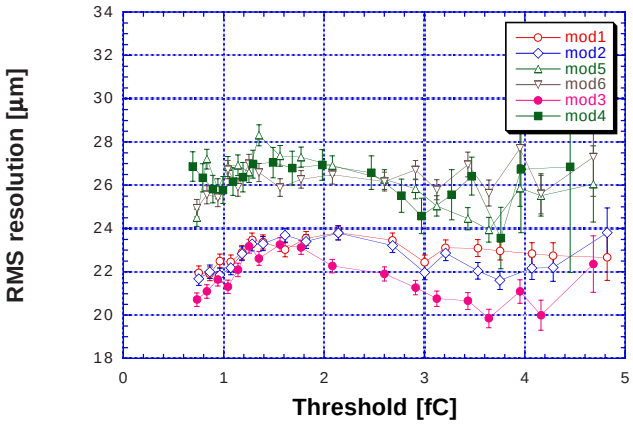

Figure 9: RMS resolutions as a function of threshold.

C. Mean cluster width

The multi-hits events had a better resolution due to the effectively narrow sensitive width. The fractions of the multi-hits, parameterized as the mean cluster width, are shown in Figure 10 and in Figure 11 as a function of bias voltage and threshold. The trends seen in the RMS resolutions can be confirmed.

D. Efficiency scans and Median charges

Counting the hits with the cluster centres within a window of the incident particles (full width of 500 µm in the analysis), an efficiency at a threshold can be obtained. Although the electronics is one threshold, the pulse height (Landau) distribution is reconstructed as an efficiency curve by scanning the threshold. Such an example is shown in Figure 12 for the irradiated module, mod3, together with the scanning of bias voltage. The threshold of the 50% efficiency is the median charge of the pulse height (Landau) distribution.

In order to obtain the threshold of 50% efficiency, a modified error function, eq. (2), was fitted to the efficiency scans,

$$eff(q) = p_3(1 - erf(T \cdot f(T))) \qquad (2)$$

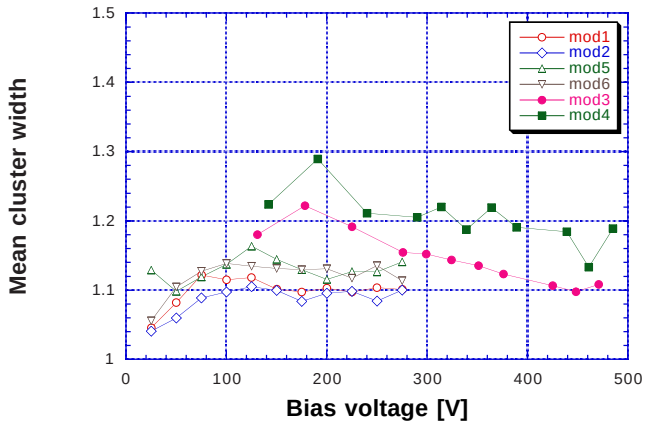

Figure 10: Mean cluster widths as a function of bias voltage

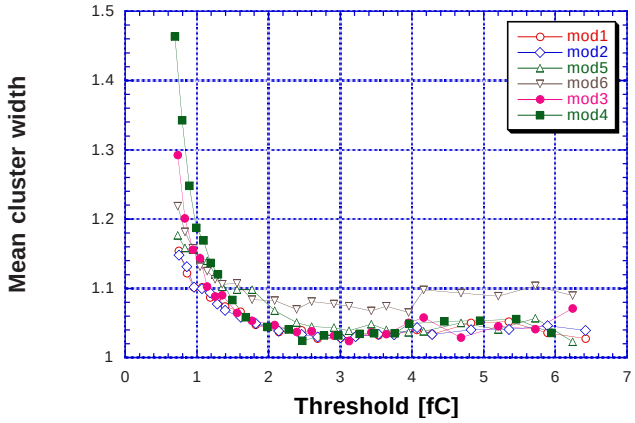

Figure 11: Mean cluster widths as a function of threshold

where

$$f(T) = 1 + 0.6 \cdot \tanh(-p_4 \cdot T) \text{ and} \quad (3)$$

$$T = (q - p_1)/(\sqrt{2} \cdot p_2). \quad (4)$$

The function, erf, was the integral of the Gaussian distribution. The function, $f(T)$, is an empirical function to modify the Gaussian to the Gaussian-convoluted Landau distribution. The fitting parameters expressed the median (p_1), the width (p_2), the saturation (p_3), and the skew (p_4).

The median charges of the modules obtained were shown in Figure 13 as a function of the bias voltage. The median charges of the non-irradiated modules were saturating above 150V to the charges between 3.8 fC and 4.0 fC. The saturations of the median charges of the irradiated modules were slower and reaching around 3.8 fC at 500V. The full depletion voltages of the non-irradiated and irradiated sensors were about 70 V and 300 V, respectively.

The median charges of the two non-irradiated barrel modules were not coinciding, nor those of the barrel and the forward modules. These differences would be attributed to the chip-by-chip variation of the calibration capacitance and insufficient

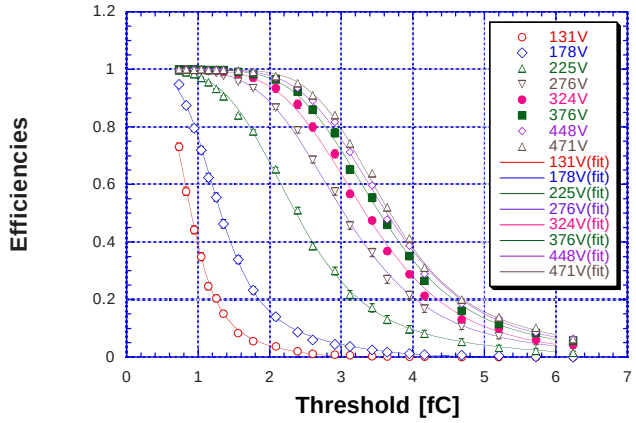

Figure 12: Threshold scan of the efficiencies at various bias voltages in the irradiated barrel module, mod3. The lines are fits to the empirical formula in the text

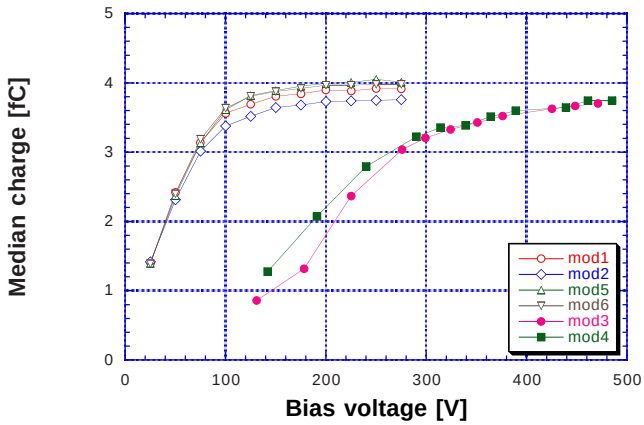

Figure 13: Bias voltage dependence of the median charges.

corrections on calibration scales due to temperature and radiation damages.

E. Noise occupancies and ENC

Noise hits due to the electronics noises were counted which were out of time (time < 15 ns) and out of track window (2*efficinecy window). The resulting number of hit strips were divided by the number of strips outside the track window, obtaining the noise occupancy. The noise occupancies of the modules are shown in Figure 14 as a function of threshold-squared. The noise occupancies at 1 fC of the non-irradiated modules were below $1x10^{-4}$ and that of the irradiated barrel module was below $1x10^{-3}$. Those of the forward modules were one order larger than of the barrel modules which would be caused by the difference in chip temperatures.

The relation between the noise occupancy and the threshold-squared is a straight line in logarithmic scale of occupancy as the occupancy is approximated as

$$occupancy(q) \propto exp(-(1/2)(q/\sigma)^2) \quad (5)$$

where σ is the equivalent-noise-charge (ENC) of the amplifiers.

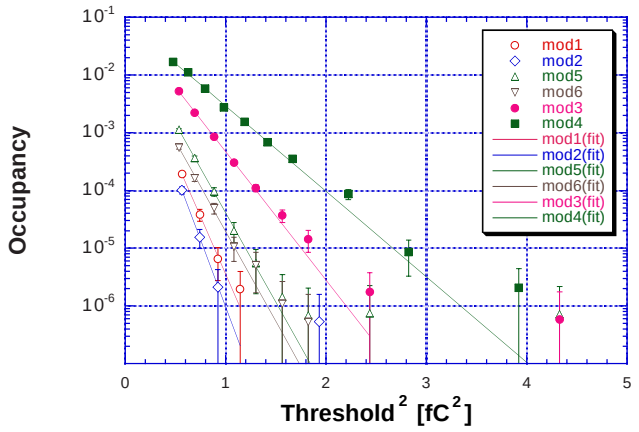

Figure 14: Noise occupancies as a function of (threshold)^2. The lines are fits to the function, exp(-1/2*(th/σ)^2)

The resulting ENCs of the modules had little bias voltage dependence. The averaged ENCs above 100 V (non-irrad) and 300 V (irrad), occuENC, are summarized in Table 4. The ENCs were obtained separately in the in-situ calibration, calibENC, with an average of ENCs at 1, 2, and 3fC, including the corrections in the section III.C. In comparison, calibENCs were systematically larger than occuENCs, which source is yet to be understood.

Table 4
Comparison of ENCs obtained from the occupancy and the in-situ calibration

mod	occuENC[fC]	calibENC[fC]	Ratio
1	0.239	0.245	0.976
2	0.222	0.234	0.949
3	0.311	0.342	0.910
4	0.385	0.411	0.937
5	0.264	0.291	0.907
6	0.264	0.290	0.910

F. Signal-to-Noise ratios

One way of cancelling the uncertainty of the calibration capacitance is to take the ratio of the median charges to the ENCs, the signal-to-noise ratios (S/N). The S/N ratio is also an indicator of the performance where S/N > 9 would be the minimum in practical use from experience. In order to calculate the S/N, the worse ENCs, calibENC, were used for conservative reason. The resulting S/N ratios are shown in Figure 15 as a function of bias voltage.

A good matching of the S/N was seen between the two barrel and two forward modules, which supported the differences of the median charges were caused by the chip-to-chip variation of the calibration capacitance. The S/N > 16 was reached above 150 V in the non-irradiated barrel, and the S/N > 10 above 300 V in the irradiated barrel modules. The S/N of forward modules were considerably lower than those of barrel modules, which would be caused by the higher chip temperatures.

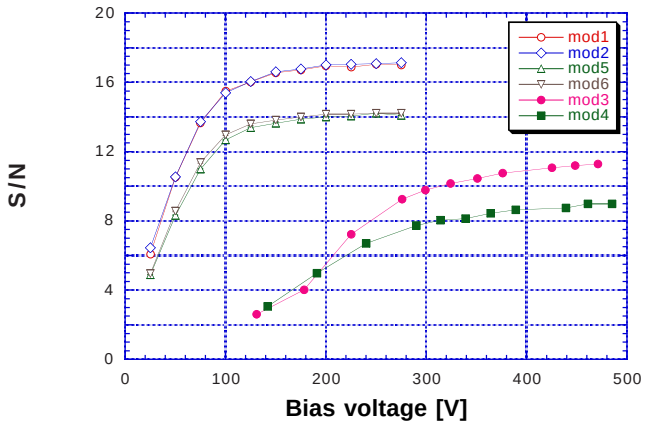

Figure 15: Signal-to-noise ratios as a function of bias voltage. The noises were averages of 1, 2, and 3 fC of the in-situ calibration

G. Charge collection in the midway regions

Since the charges moving in the midway between two strips generate currents in both strips, the charges induced are halved, and thus the efficiency would be deteriorated. This is seen in Figure 16 by mapping the regions between two strips, where “eta” is the normalized distance from the strips. Degradations were seen in high thresholds, however, the efficiencies were still high at 1 fC. The ratios of the median charges in the strip and the midway region were about 0.95 and 0.85 in the non-irradiated and the irradiated modules. The thresholds where the loss of efficiency starts could be estimated by applying these factors to the efficiency curves, e.g., in Figure 12.

H. Common-mode noises

If the electronics system has an external noise pick-up or an internal oscillation, the noise appears as a multiple hits of the strips, a common-mode noise. The distributions of number of hits in the non-irradiated (average of mod1 and mod2) and irradiated (mod3) modules are shown in Figure 17 at the threshold of 0.7 fC. No excess tail of a common-mode noise was observed.

V. SUMMARY

Two beamtests were carried out by using 4 GeV/c pions from the 12 GeV proton synchrotron at KEK for the ATLAS SCT barrel and forward modules fully equipped with the SCT specification components, including the modules irradiated to a fluence of 3x10^{14} protons/cm^2, the equivalent fluence expected in the operation of 10 years in the ATLAS detector at LHC.

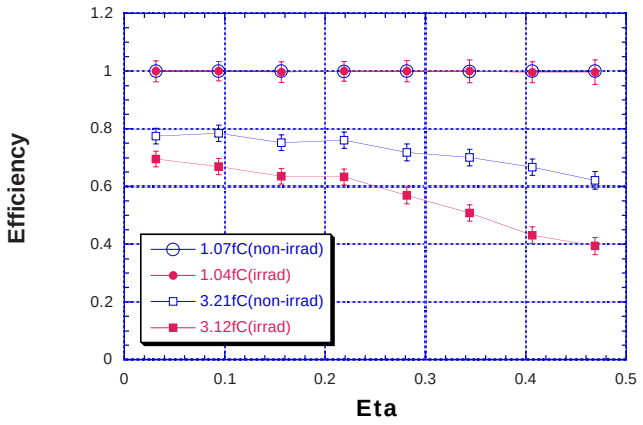

Figure 16: Efficiencies between the strips. “Eta” defines the distance from the strips: 0 at strip and 0.5 at midway.

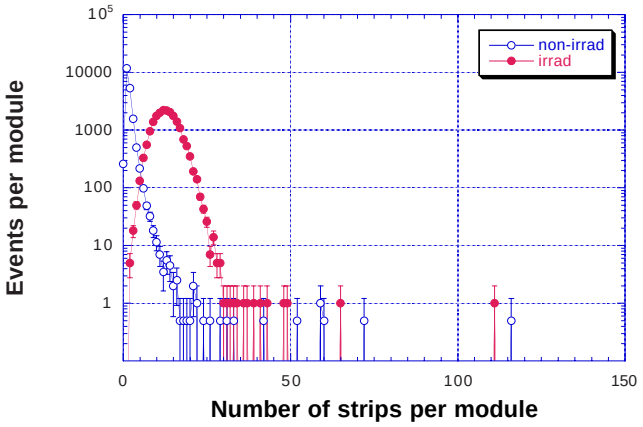

Figure 17: Distribution of the number of strips hit in the non-irradiated (average of mod1 and mod2) and irradiated (mod3) modules at 0.7 fC thresholds

The pulse shape analysis confirmed the peaking time of the amplifier to be 22 ns in the non-irradiated modules and deteriorated to 27 ns in the irradiated modules. An excess shoulder in the pulse shapes was observed which would be a feedback of the discriminator shocks.

The RMS position resolutions were consistent with the uniform distribution of the pitch of 80 μm in the barrel and of 86 μm in the forward where the beam spot was. The variations of the resolutions were correlated to the fraction of the multi-hits events in the midway between the strips which gave much better resolutions.

Scanning of the threshold of the on-off readout, the median charges of the pulse height (Landau) distribution were obtained which saturated around 3.8 fC in the non-irradiated (>150 V) and irradiated (500 V) modules.

The noise occupancies at 1 fC were below $1x10^{-4}$ in the non-irradiated and below $1x10^{-3}$ in the irradiated barrel modules. The ENCs obtained from the noise occupancies were systematically lower than those obtained from the in-situ calibration, which requires further investigation to understand.

Using the median charges and the ENCs of in-situ calibration, the signal-to-noise ratios were >16 in the non-irradiated (>150 V) and >10 in the irradiated (>300 V) barrel modules. The matching of the S/N of the non-irradiated barrel modules indicated the spread of the median charges were caused by the variation of the chip-by-chip calibration capacitance.

The forward modules showed deterioration in two areas: (1) rise times of the pulses and larger excess shoulders, and (2) ENCs. These would be associated to much higher temperatures of the readout ASICs.

No excess common-mode was observed in the beamtests.

VI. Acknowledgement

The authors wish to acknowledge the cooperation of the beam channel crews of the d π2 beamline of the KEK PS and support from the ATLAS SCT collaboration.

VII. References

[1] Y. Unno, “ATLAS silicon microstrip Semiconductor Tracker (SCT), Nucl. Instr. Metho. A453, pp.109-120, 2000

[2] ATLAS Inner Detector Technical Design Report, CERN/LHCC/97-17, ATLAS TDR 5, 30 April 1997

[3] Y. Unno et al., (1) Testbeam experiment T450, KEK, 10-20 Dec. 1999, (2) Testbeam experiment T478, KEK, 28 Nov.-10 Dec. 2000

[4] Y. Unno et al., “Evaluation of Radiation Damaged P-in-n and N-in-n Silicon Microstrip Detectors”, IEEE Trans. Nucl. Scie., Vol. 46, pp. 1957-1963, 1999

[5] Sensors fabricated by Hamamatsu Photonics, 1126-1, Ichino-cho, Hamamatsu-shi 435, Japan

[6] DMILL technology, TEMIC Semiconductors, La Chantrerie, F-44306 Nantes, France

[7] F. Anghinolfi et al., “Performance of the Electrical Module Prototypes for the ATLAS Silicon Tracker”, Snowmass 1999, Electronics for LHC experiments, pp. 118-122

[8] W. Dabrowski et al., “Design and Performance of the ABCD Chip for the Binary Readout of Silicon Strip Detectors in the ATLAS Semiconductor Tracker”, IEEE Trans.Nucl.Sci. Vol. 47, pp. 1843-1850, 2000

[9] The FR-, VAL-, and CG-modules were prepared by Univ. Freiburg, Univ. Valencia, and CERN-Univ. Geneva, respectively. The rest of the modules were by KEK

[10]W. Dabrowski, private communication